Heliyon 10 (2024) e36726

Contents lists available at ScienceDirect

Heliyon

journal homepage: www.cell.com/heliyon

Research article

Hepatic Dyrk1b impairs systemic glucose homeostasis by modulating Wbp2 expression in a kinase activity-dependent manner

Lianju Li [a,b,*], Yaoyu Zou [c], Chongrong Shen [a,b], Na Chen [a,b], Muye Tong [a,b], Ruixin Liu [a,b], Jiqiu Wang [a,b,**], Guang Ning [a,b,***]

[a] Department of Endocrine and Metabolic Diseases, Shanghai Institute of Endocrine and Metabolic Diseases, Ruijin Hospital, Shanghai Jiao Tong University School of Medicine, Shanghai, 200025, China
[b] Shanghai National Clinical Research Center for Metabolic Diseases, Key Laboratory for Endocrine and Metabolic Diseases of the National Health Commission of the PR China, Shanghai National Center for Translational Medicine, Shanghai, 200025, China
[c] Shanghai Ji Ai Genetics & IVF Institute, Obstetrics & Gynecology Hospital, Fudan University, Shanghai, 200025, China

ARTICLE INFO

Keywords:
Glucose tolerance
Insulin resistance
Glucose homeostasis
Dyrk1b
Wbp2
Type 2 diabetes

ABSTRACT

Patients with gain-of-function mutations of Dyrk1b have higher fasting blood glucose (FBG) levels. However, the role of Dyrk1b in glucose metabolism is not fully elucidated. Herein, we found that hepatic Dyrk1b overexpression in mice impaired systemic glucose tolerance and hepatic insulin signaling. Dyrk1b overexpression in vitro attenuated insulin signaling in a kinase activity-dependent manner, and its kinase activity was required for its effect on systemic glucose homeostasis and hepatic insulin signaling in vivo. Dyrk1b ablation improved systemic glucose tolerance and hepatic insulin signaling in mice. Quantitative proteomic analyses showed that Dyrk1b downregulated WW domain-binding protein 2 (Wbp2) protein abundance. Mechanistically, Dyrk1b enhanced Wbp2 ubiquitylation and proteasomal degradation. Restoration of hepatic Wbp2 partially rescued the impaired glucose homeostasis in Dyrk1b overexpression mice. In addition, Dyrk1b inhibition with AZ191 moderately improved systemic glucose homeostasis. Our study uncovers that hepatic Dyrk1b impairs systemic glucose homeostasis via its modulation of Wbp2 expression in a kinase activity-dependent manner.

1. Introduction

The prevalence of diabetes mellitus has continued to rise over the past 50 years. Increase in the incidence of type 2 diabetes (T2D) is a driver of the global epidemic of diabetes mellitus [1]. As a heterogeneous metabolic disorder, T2D is characterized by insufficient insulin secretion in the context of insulin resistance [1]. T2D and its intractable complications contribute enormously to the global

* Corresponding author. Department of Endocrine and Metabolic Diseases, Shanghai Institute of Endocrine and Metabolic Diseases, Ruijin Hospital, Shanghai Jiao Tong University School of Medicine, Shanghai, 200025, China.
** Corresponding author. Department of Endocrine and Metabolic Diseases, Shanghai Institute of Endocrine and Metabolic Diseases, Ruijin Hospital, Shanghai Jiao Tong University School of Medicine, Shanghai, 200025, China.
*** Corresponding author. Department of Endocrine and Metabolic Diseases, Shanghai Institute of Endocrine and Metabolic Diseases, Ruijin Hospital, Shanghai Jiao Tong University School of Medicine, Shanghai, 200025, China.
E-mail addresses: 215977459@qq.com (L. Li), wangjq@shsmu.edu.cn (J. Wang), ningguang@sjtu.edu.cn (G. Ning).

https://doi.org/10.1016/j.heliyon.2024.e36726
Received 22 May 2024; Received in revised form 5 August 2024; Accepted 21 August 2024
Available online 22 August 2024

burden of disability and mortality [2]. The research of T2D has been accelerated by advancements in human genetics, mechanistic studies, epigenetics, and clinical trials, providing new insights into the genetic predisposition, pathophysiology, and treatment of this condition [3]. The maintenance of glucose homeostasis is essential and is achieved through a complex control of glucose utilization and production. Tissues critical for glucose homeostasis include the liver, muscle, fat, and brain [4]. In particular, the liver plays a central role in glucose homeostasis by balancing glucose storage via glycogenesis and glucose production via glycogenolysis and gluconeogenesis [4]. Excessive hepatic glucose production in patients with T2D impairs glucose homeostasis and contributes to hyperglycemia [5]. Glucose-lowering therapy remains a mainstay of T2D treatment [6,7]. Elucidation of the mechanisms controlling glucose homeostasis may deepen our understanding of the pathogenesis of T2D and expand our armamentarium of drugs for more specific and tailored treatment of T2D in the future.

Dyrk1b (also known as Mirk) is a member of the evolutionarily conserved Dyrk/Minibrain family of arginine-directed serine/threonine protein kinases. Mammalian Dyrks (dual-specificity tyrosine phosphorylation-regulated kinases) fall into two subgroups, class I (Dyrk1a and Dyrk1b) and class II (Dyrk2, Dyrk3 and Dyrk4) [8]. Dyrks possess a tyrosine-X-tyrosine residue motif in the activation loop and autophosphorylation of the second tyrosine residue is important for kinase activity [9]. Dyrks exclusively phosphorylate serine or threonine residues on their substrates [10]. Of note, growing evidence has shown that Dyrk1b is a pleiotropic protein. For instance, Dyrk1b enables MEF2C to transcribe the muscle regulatory factor *myogenin* by phosphorylating and decreasing the nuclear localization of class II histone deacetylases [11]. Dyrk1b functions as a survival factor in differentiating myoblasts [12], rhabdomyosarcomas [13], and pancreatic ductal adenocarcinoma [14]. Dong et al. uncover Dyrk1b as an effector mediating transcription silencing on damaged chromatin and a suppressor of ribosomal DNA transcription during cellular response to DNA damage [15,16]. There is ample evidence that Dyrk1b expression is elevated in several solid tumors, such as osteosarcoma [17], lung cancer [18], and triple-negative breast cancer [19] and that depletion or inhibition of Dyrk1b may be a potential therapeutic target for these tumors [20,21].

Our group has recently identified Dyrk1b as an important modulator in platelet production and cardiac hypertrophy [22,23]. Dyrk1b expression is upregulated during cardiac hypertrophy and heart failure [23]. Dyrk1b promotes phosphorylation and nuclear accumulation of STAT3, leading to PGC-1α downregulation and impaired mitochondrial bioenergetics and cardiac dysfunction. Pharmacological inhibition of Dyrk1b with AZ191 shows therapeutic benefits against cardiac hypertrophy in mice [8,23]. Importantly, using linkage analysis and whole-exome sequencing in three families with coinheritance of early-onset artery disease, hypertension, central obesity, and diabetes, Keramati and colleagues identify a founder p.R102C mutation in Dyrk1b shared in the affected family members [24]. Functional characterization indicates that Dyrk1b not only enhances adipogenesis by inhibiting the sonic hedgehog and Wnt signaling pathways, but also promotes expression of glucose-6-phosphatase, a key gluconeogenic enzyme [24]. The p.R102C mutation presents gain-of-function activity and family members carrying Dyrk1b p.R102C mutation have significantly higher fasting blood glucose levels compared to non-carriers [24]. These instructive findings imply the role of Dyrk1b in glucose metabolism and prompt us to explore its role in glucose homeostasis.

In the present study, we investigated whether Dyrk1b could regulate glucose metabolism mainly by evaluating the glucose metabolic phenotypes of mice with hepatic Dyrk1b overexpression and mice with Dyrk1b knockout. Furthermore, we elucidated the underlying mechanisms of Dyrk1b in the regulation of glucose homeostasis through proteomic analyses.

2. Materials and methods

2.1. Animals

C57BL/6J (hereafter referred to as C57) mice were purchased from Shanghai Jihui Laboratory Animals Care Co., Ltd. *Dyrk1b* knockout (*Dyrk1b*$^{-/-}$) mice were generated using the transcription activator-like effector nuclease (TALEN) strategy as previously described [23,25]. Mice were maintained in a temperature-controlled facility with a 12-h light/dark cycle and given free access to food and water. All animal studies were conducted in accordance with the guidelines for animal care and approved by the Animal Care Committee of Shanghai Jiao Tong University School of Medicine (approval number: B-2016-016).

2.2. Adenovirus

Adenoviruses expressing mouse Dyrk1b (NM_001037957) (Ad-Dyrk1b), mouse Wbp2 (NM_016852) (Ad-Wbp2), and control EGFP (Ad-EGFP) were generated using the AdMaxTM adenoviral vector system (Shanghai Genechem Co., Ltd.) as previously described [26]. To overexpress Dyrk1b or Wbp2 in mouse liver, 1.5×10^9 plaque-forming units (PFU) of adenovirus in 150 μL PBS was injected into mice via tail vein. To overexpress kinase-defective Dyrk1b in mouse liver, 7.5×10^9 PFU of adenovirus was injected into mice via tail vein.

2.3. Metabolic evaluation

As described in previous studies [27,28], for glucose tolerance test (GTT), mice were fasted for 16 h and subsequently injected intraperitoneally with glucose (2 g/kg b.w.). Mice were subjected to fast for 6 h and injected intraperitoneally with insulin (0.75 IU/kg b.w.) for insulin tolerance test (ITT). Pyruvate tolerance test (PTT) were performed on mice fasted for 16 h. Mice were given sodium pyruvate (1 g/kg b.w.) intraperitoneally. In GTT, ITT, and PTT, tail blood glucose levels were measured with glucometers before and at

15, 30, 60, 90, and 120 min after injection of glucose, insulin or sodium pyruvate. Mice were sacrificed following fasting for 6 h. Plasma and tissues of mice were then collected and stored at −80 °C for further analysis. Plasma parameters, including Aspartate Transaminase (AST), Triglyceride (TG), Total Cholesterol (TC), High-density Lipoprotein Cholesterol (HDL-C), and Low-density Lipoprotein Cholesterol (LDL-C) were measured using commercially available kits according to the manufacturer's instructions (Kehua Bio-Engineering, Shanghai, China) [29,30]. Briefly, for the measurement of plasma AST, the mixed reagents were added to the samples. After incubation at 37 °C, the absorbance at 340 nm was measured continuously for 3 min to calculate the AST concentration. To measure plasma TG, the mixed reagents were added to the samples and the TG standard. After incubation at 37 °C for 5 min, the absorbance at 550 nm was measured to calculate the TG concentration. For the measurement of plasma TC, the mixed reagents were added to the samples and the TC standard. After incubation at 37 °C for 5 min, the absorbance at 546 nm was measured to calculate the TC concentration. To measure plasma HDL-C, reagent R1 was added to the samples and the HDL-C standard. After incubation at 37 °C for 5 min, reagent R2 was then added. After incubation at 37 °C for 1 min, the absorbance at 600 nm was measured continuously for 3 min to calculate the HDL-C concentration. To measure plasma LDL-C, after the detection reagents were added to the samples and the LDL-C standard, the absorbance at 600 nm was measured to calculate the LDL-C concentration.

2.4. Cell experiments

Mouse Hepa1-6 hepatoma cells (CRL-1830; ATCC) were cultured in Dulbecco's modified Eagle's medium (DMEM) (11995040; Gibco) containing 10 % fetal bovine serum (FBS) (16140071; Gibco) and 1 % penicillin/streptomycin (15140122; Gibco). To investigate the effect of Dyrk1b overexpression in vitro, Hepa1-6 cells were infected with Ad-Dyrk1b (3×10^{10} PFU/ml) or Ad-EGFP (3×10^{10} PFU/ml) at an multiplicity of infection (MOI) of 100.

2.5. Glucose uptake

Glucose uptake of cells was measured using the Glucose Uptake-Glo™ Assay (J1341; Promega) according to the manufacturer's instructions [31]. After removing the medium and washing with PBS, the prepared 2-deoxyglucose (2DG) was added to cells and then incubated for 10 min at room temperature. Stop buffer, neutralization buffer, and 2-deoxyglucose-6-phosphate (2DG6P) detection reagent were added sequentially and incubated for 1 h at room temperature. Luminescence was recorded.

2.6. RT-qPCR

Total RNA was extracted using RNA extraction kit (LS1040; Promega) in accordance with our previous study [32]. cDNA was then synthesized with PrimeScript™ RT Master Mix (RR036A; Takara). Real-time quantitative PCR was performed with SYBR Green Master Mix (Q711; Vazyme). 36B4 or β-actin served as the reference gene and the relative expression of genes was calculated using the $2^{-\Delta\Delta CT}$ method [33]. Primer sequences for RT-qPCR are provided in Table S1.

2.7. Western blot

As previously described [34], tissues or cells were homogenized in RIPA lysis buffer (R20095; Biocolor) supplemented with protease and phosphatase inhibitors (78441; Thermo Fisher). Equal amounts of protein were fractionated on 10 % SDS-PAGE gels and transferred to polyvinylidene difluoride (PVDF) membranes. The membranes were incubated with primary antibodies and horseradish peroxidase-conjugated secondary antibodies. Antibodies against Dyrk1b (5672; CST), p-Akt (Thr308) (9275; CST), p-Akt (Ser473) (4060; CST), Akt (9272; CST), Wbp2 (11831S; CST), Ddx49 (sc-514928; Santa Cruz), and Hsp90 (4877; CST) were used. Protein levels were quantified using Image J and normalized to Hsp90.

2.8. Cycloheximide (CHX) chase assay

CHX chase assays were performed to determine the half-life of Wbp2 [35]. In brief, Hepa1-6 cells were infected with Ad-EGFP or Ad-Dyrk1b for 24 h and then treated with cycloheximide (20 μg/ml) for different time periods. The protein lysate was harvested at the indicated time points and then Western blot was performed to determine the half-life of Wbp2.

2.9. Immunoprecipitation

Hepa1-6 cells were cotransfected with Dyrk1b-HA, Wbp2-Flag, and Ubiquitin (Ub)-Myc expression vectors using Lipofectamine 3000 transfection reagent (L3000015, Thermo Fisher) [36]. Two days after transfection, immunoprecipitation was performed with commercial kits (88804; Thermo Fisher) [37]. Cells were harvested and lysed with IP buffer supplemented with protease inhibitor. Pierce Protein A/G Magnetic Beads were incubated with Flag antibody (F1804; Sigma) for 4 h at 4 °C, and then the antibody-beads and lysate complex were incubated overnight at 4 °C. After washing, the eluted protein was analyzed by Western blot.

2.10. Liver TG

Triglyceride (TG) levels in liver tissues were measured using commercial kits (K622-100, BioVision, USA) according to the manufacturer's instructions, as previously described [38]. Briefly, frozen livers were homogenized in 5 % NP-40 buffer and slowly heated to 100 °C for 5 min. After repeating the heating again, the samples were centrifuged for 2 min to collect the supernatant. 50 μL samples and TG standard were added to a 96-well plate. 2 μL lipase was added to each well and incubated at room temperature for 20 min. 50 μL triglyceride reaction mix was added to each well and incubated at room temperature for 60 min. After measuring the absorbance at 570 nm, the standard curve was plotted to calculate the TG concentration of the samples.

2.11. Hepatocyte isolation

A modified collagenase method was used to isolate primary hepatocytes [36]. In brief, after the mice were anesthetized, the liver was perfused with EGTA buffer and then with collagenase buffer for cell dissociation. The liver was then excised, minced, and filtered through a 100 mm steel mesh. Primary hepatocytes were centrifuged at 50 *g* for 5 min and cultured in DMEM supplemented with 10 % FBS and 1 % penicillin/streptomycin.

2.12. TMT quantitative proteomic analyses

(TMT)-based quantitative proteomic analysis was performed to identify potential targets of Dyrk1b [39]. Briefly, livers were suspended in lysis buffer (4 % SDS, 100 mM DTT, 150 mM Tris-HCl pH 8.0) and disrupted with a homogenizer. After boiling, the samples were ultrasonicated and boiled again. The protein supernatant was collected and quantified. Protein digestion was performed according to the FASP procedure [40]. The digested peptides were collected as a filtrate and concentration was determined. Peptides were labeled with TMT reagents according to the manufacturer's instructions (Thermo Fisher). A Pierce high pH reversed-phase fractionation kit (Thermo Fisher) was used to fractionate TMT-labeled samples. The peptide content of each fraction was evaporated to dryness and used for LC-MS analysis. LC-MS/MS analysis was performed and the resulting LC-MS/MS raw files were imported into MaxQuant (version 1.6.0.16) for data interpretation and protein identification. The proteomic raw data have been deposited to the ProteomeXchange Consortium with the dataset identifier PXD042393.

2.13. Statistical analysis

For each experiment, the sample size, statistical test, and significance threshold could be found in the figure legends. All statistical analyses were performed with Prism 10.2.0 (GraphPad Software). Data were presented as mean ± SEM. Differences between two groups were determined by Student's t-test. One-way ANOVA followed by Tukey's post-hoc test was used for comparisons of differences among more than two groups. Two-way ANOVA followed by an appropriate post-hoc test was used for data from a 2×2 factorial design. P values < 0.05 were considered statistically significant.

3. Results

3.1. Hepatic Dyrk1b overexpression impairs glucose tolerance and liver insulin sensitivity

To assess whether hepatic Dyrk1b affects systemic glucose homeostasis, adenovirus expressing mouse Dyrk1b (Ad-Dyrk1b) or control adenovirus (Ad-EGFP) was injected into female mice on a NCD (Fig. 1a). Hepatic Dyrk1b overexpression resulted in higher fasting blood glucose (FBG) and glucose levels after glucose injection in GTT and higher AUC of GTT, indicating impaired systemic glucose tolerance (Fig. 1b and c). Insulin tolerance test (ITT) revealed impaired insulin tolerance caused by hepatic Dyrk1b overexpression (Fig. 1d and e). In pyruvate tolerance test (PTT), Dyrk1b overexpression led to elevated blood glucose levels following pyruvate challenge (Fig. 1f). In addition, Dyrk1b overexpression led to increased liver weights (Fig. S1a) and triglyceride (TG) contents (Fig. 1g). The increase in hepatic TG contents caused by Dyrk1b overexpression is consistent with the findings of Bhat et al [41]. Furthermore, Dyrk1b overexpression mice showed decreased levels of insulin-stimulated p-Akt at both Thr308 and Ser473 in liver (Fig. 1h–k), indicating attenuated hepatic insulin signaling. The mRNA levels of *Gys2* and *Acaca* were decreased in livers of Dyrk1b overexpression mice (Fig. S1b). However, there were no differences in mRNA levels of *Fasn*, *Srebf1*, *Pygl*, *Acox1*, *Acadm*, or *Pnpla2* between the two groups (Fig. S1b).

Similarly, hepatic Dyrk1b overexpression in male mice led to fasting hyperglycemia and exacerbation of systemic glucose tolerance in GTT (Figs. S2a–c). These Dyrk1b overexpression mice also had elevated FBG levels in ITT (Fig. S2d). However, the differences of the glucose levels after insulin administration were not statistically significant (Fig. S2d). Significantly increased liver TG contents (Fig. S2e) and lower liver p-Akt at both Thr308 and Ser473 were also observed when Dyrk1b was overexpressed in male mice (Figs. S2f–i). Taken together, these data demonstrate that hepatic Dyrk1b overexpression impairs systemic glucose tolerance and hepatic insulin sensitivity.

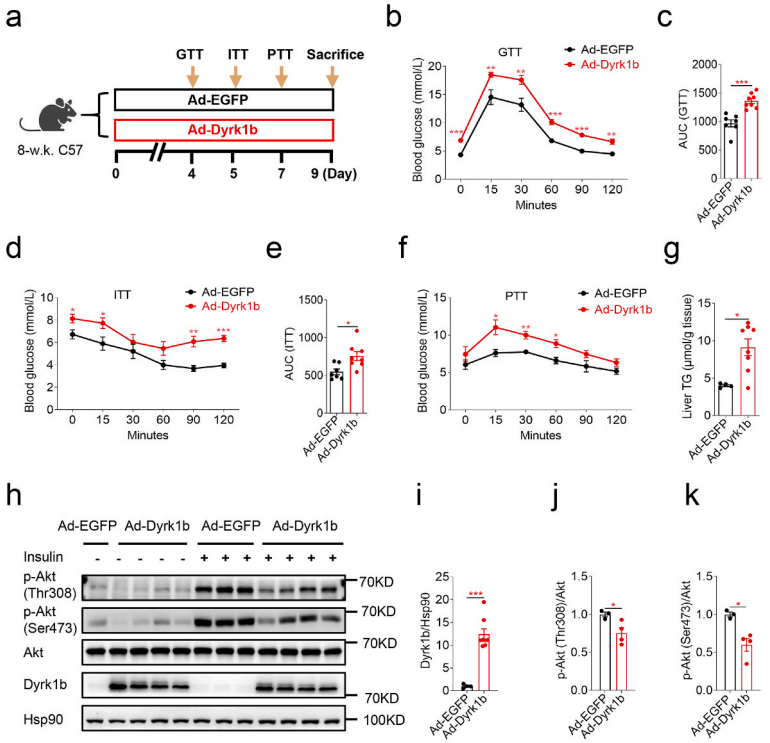

Fig. 1. Hepatic Dyrk1b overexpression impairs glucose tolerance and liver insulin sensitivity. (**a**) Experimental designs following Ad-Dyrk1b or Ad-EGFP injection of female C57 mice. Intraperitoneal glucose tolerance test (**b**) and AUC of GTT curves (**c**) of Ad-EGFP (n = 7) and Ad-Dyrk1b (n = 8) female mice. Insulin tolerance test (**d**) and AUC of ITT curves (**e**) of Ad-EGFP (n = 7) and Ad-Dyrk1b (n = 8) female mice. Pyruvate tolerance test (**f**) of Ad-EGFP (n = 5) and Ad-Dyrk1b (n = 8) female mice. Liver TG contents (**g**) of Ad-EGFP (n = 4) and Ad-Dyrk1b (n = 8) female mice. Unpaired Student's t-test (two-sided) was performed for Fig. 1**b**–**g**. (**h**–**k**) Western blot and densitometry quantification of livers from Ad-EGFP (n = 4) and Ad-Dyrk1b (n = 8) female mice. Unpaired Student's t-test (two-sided) was performed for Fig. 1**i**–**k**. *P < 0.05, **P < 0.01, ***P < 0.001.

3.2. *Dyrk1b overexpression attenuates insulin signaling in a kinase activity-dependent manner*

To further explore the cell-autonomous effects of Dyrk1b in glucose metabolism and insulin signaling, we overexpressed Dyrk1b in mouse Hepa1-6 hepatoma cells (Fig. 2a). Glucose uptake was significantly lower in cells overexpressing Dyrk1b (Fig. 2b). Consistently, insulin-stimulated p-Akt at both Thr308 and Ser473 was remarkably suppressed in Hepa1-6 cells overexpressing Dyrk1b (Fig. 2c–e). Importantly, the attenuated insulin signaling due to Dyrk1b overexpression was restored by treatment with AZ191 [8], a potent and selective inhibitor of Dyrk1b (Fig. 2f and g). Moreover, in contrast to wild-type Dyrk1b, kinase-defective Dyrk1b with Y271/273F mutation [24] failed to inhibit insulin signaling (Fig. 2h–j). These data suggest that Dyrk1b inhibits insulin signaling in a kinase activity-dependent manner.

To further test whether the kinase activity of Dyrk1b was required for its role in glucose tolerance and insulin sensitivity in vivo, adenovirus expressing kinase-defective Dyrk1b was injected into female mice (Fig. 2k). Compared to wild-type Dyrk1b, kinase-defective Dyrk1b did not impair systemic glucose tolerance or insulin sensitivity of mice (Fig. 2l–o). Western blotting showed that kinase-defective Dyrk1b did not attenuate hepatic insulin signaling (Fig. 2p–r). These results highlight the requirement of Dyrk1b kinase activity for its function in glucose homeostasis in vivo.

3.3. *Dyrk1b ablation improves systemic glucose tolerance and hepatic insulin signaling*

Given the aforementioned deleterious glucose metabolism caused by Dyrk1b overexpression in vivo and in vitro, we next examined whether global Dyrk1b ablation could improve glucose metabolism. As expected, in the GTT, female *Dyrk1b*$^{-/-}$ mice on a NCD were more glucose tolerant than control littermates (Fig. 3a–c). However, Dyrk1b ablation had no effect on systemic insulin sensitivity (Fig. 3d) or pyruvate tolerance (Fig. S3a). Liver weights were lower in female *Dyrk1b*$^{-/-}$ mice (Fig. S3b), although liver TG contents were comparable between the two groups (Fig. S3c). Importantly, female *Dyrk1b*$^{-/-}$ mice displayed significantly enhanced levels of insulin-induced p-Akt at both Thr308 and Ser473 in the livers (Fig. 3e–g). We also examined p-Akt in quadriceps muscles and no

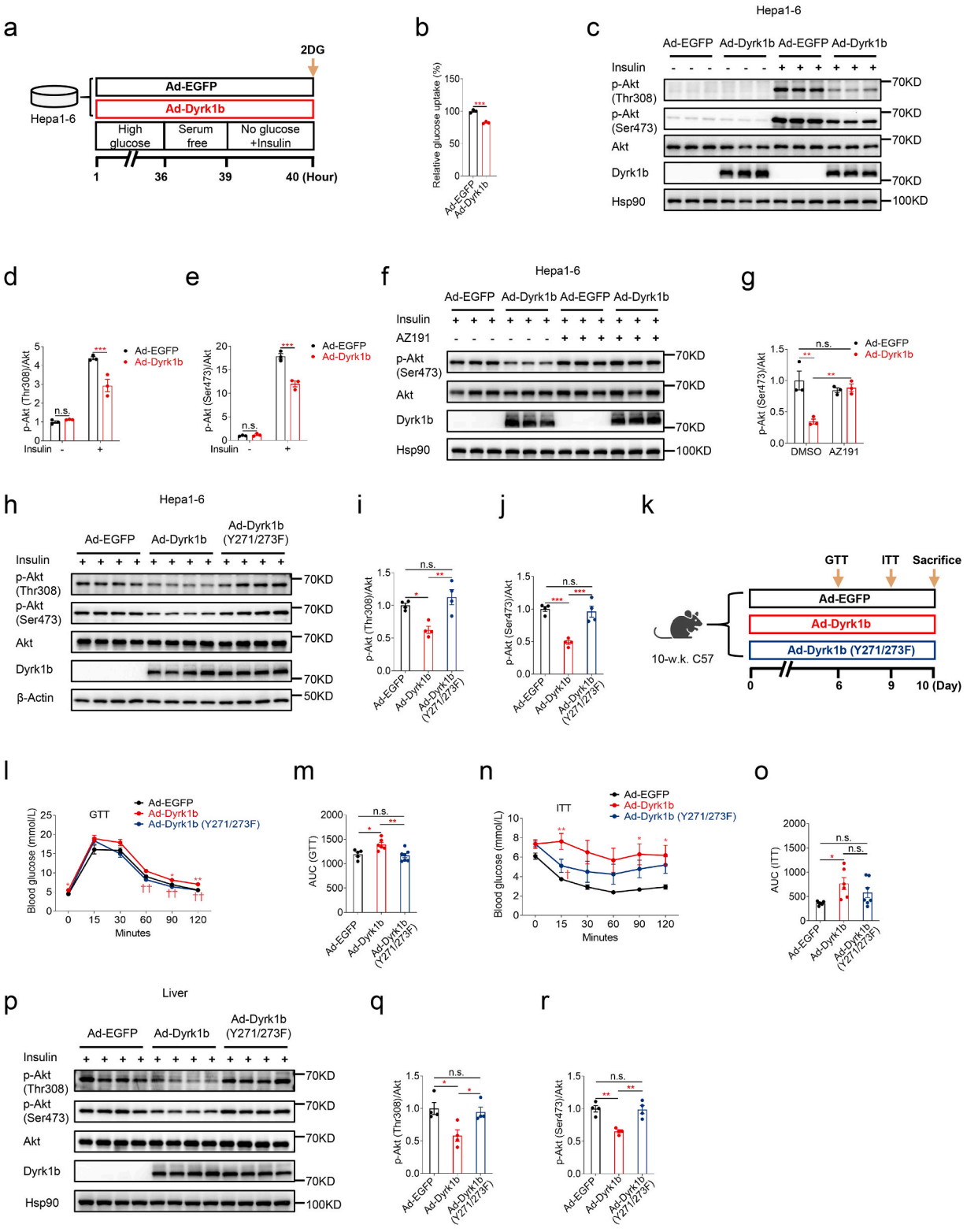

(caption on next page)

Fig. 2. Dyrk1b overexpression attenuates insulin signaling in a kinase activity-dependent manner. (**a**) Experimental designs following Ad-Dyrk1b or Ad-EGFP infection of Hepa1-6 cells. (**b**) Glucose uptake of Hepa1-6 cells infected with Ad-EGFP or Ad-Dyrk1b (MOI = 100) (n = 3). Unpaired Student's t-test (two-sided) was performed for Fig. 2**b**. (**c**–**e**) Western blot and densitometry quantification of Hepa1-6 cells infected with Ad-EGFP or Ad-Dyrk1b (MOI = 100) (n = 3). Two-way ANOVA with Sidak's post-hoc test was performed for Fig. 2**d** and **e**. (**f**–**g**) Western blot and densitometry quantification of Hepa1-6 cells infected with Ad-EGFP or Ad-Dyrk1b in the absence or presence of AZ191 (1 μM) (n = 3). Two-way ANOVA with Tukey's post-hoc test was performed for Fig. 2**g**. (**h**–**j**) Western blot and densitometry quantification of Hepa1-6 cells infected with adenovirus expressing wild-type Dyrk1b or kinase-defective Dyrk1b with Y271/273F mutation. One-way analysis of variance (ANOVA) with Tukey's post-hoc test was performed for Fig. 2**i** and **j**. (**k**) Experimental designs for female C57 mice injected with adenovirus expressing wild-type or kinase-defective Dyrk1b. Intraperitoneal glucose tolerance test (**l**) and AUC of GTT curves (**m**) of mice injected with adenovirus expressing wild-type or kinase-defective Dyrk1b (n = 5–7). Insulin tolerance test (**n**) and AUC of ITT curves (**o**) of mice injected with adenovirus expressing wild-type or kinase-defective Dyrk1b (n = 6–7). One-way ANOVA with Tukey's post-hoc test was performed for Fig. 2**l**–**o**. *P < 0.05 and **P < 0.01 for mice injected with Ad-EGFP versus Ad-Dyrk1b. †P < 0.05 and ††P < 0.01 for mice injected with Ad-Dyrk1b versus Ad-Dyrk1b (Y271/273F). (**p**–**r**) Western blot and densitometry quantification of livers from mice injected with adenovirus expressing wild-type or kinase-defective Dyrk1b (n = 4). One-way ANOVA with Tukey's post-hoc test was performed for Fig. 2**q** and **r**. *P < 0.05, **P < 0.01, ***P < 0.001, n.s., not significant.

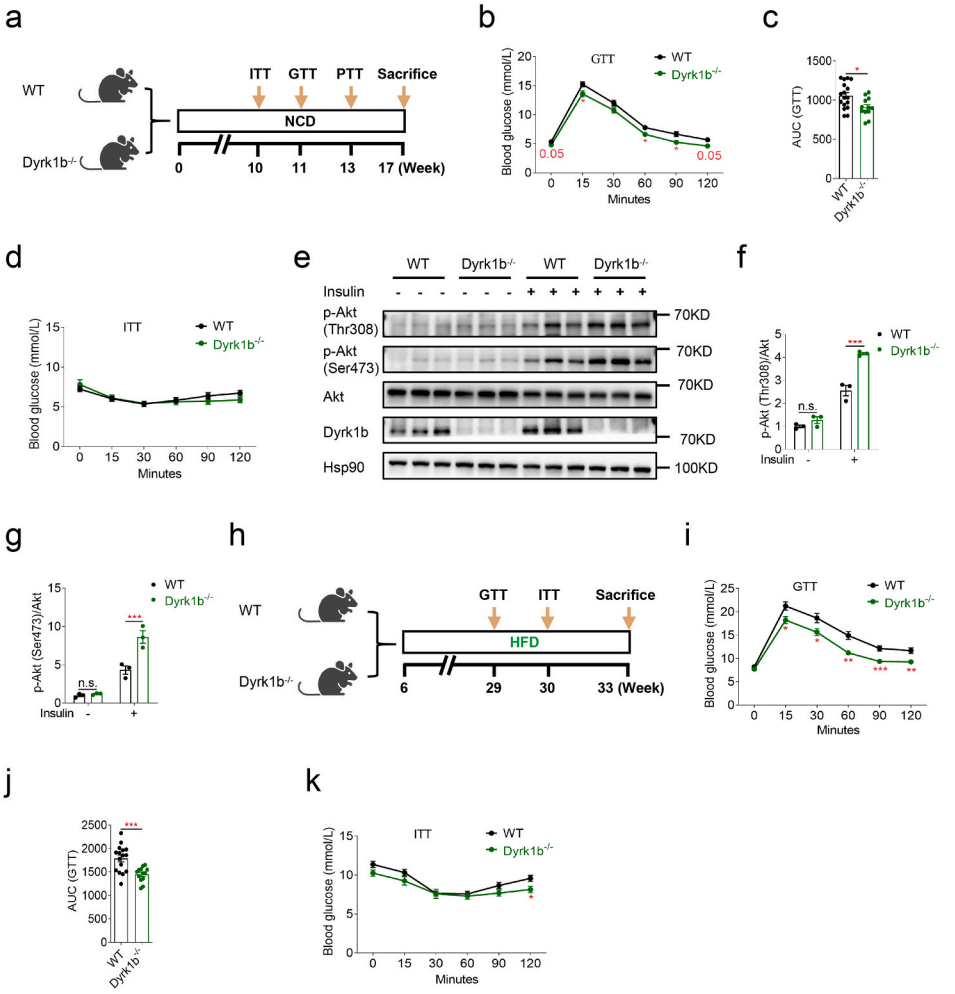

Fig. 3. Dyrk1b ablation improves systemic glucose tolerance and hepatic insulin signaling. (**a**) Experimental designs for WT and *Dyrk1b*$^{-/-}$ female mice on a NCD. Intraperitoneal glucose tolerance test (**b**), AUC of GTT curves (**c**), and insulin tolerance test (**d**) of WT (n = 17) and *Dyrk1b*$^{-/-}$ (n = 12) female mice on a NCD. Unpaired Student's t-test (two-sided) was performed for Fig. 3**b**–**d**. (**e**–**g**) Western blot and densitometry quantification of livers from WT and *Dyrk1b*$^{-/-}$ female mice on a NCD (n = 3). Two-way ANOVA with Sidak's post-hoc test was performed for Fig. 3**f** and **g**. (**h**) Experimental designs for WT and *Dyrk1b*$^{-/-}$ male mice on a HFD. Intraperitoneal glucose tolerance test (**i**), AUC of GTT curves (**j**), and insulin tolerance test (**k**) of WT (n = 16) and *Dyrk1b*$^{-/-}$ (n = 12) male mice on a HFD. Unpaired Student's t-test (two-sided) was performed for Fig. 3**i**–**k**. *P < 0.05, **P < 0.01, ***P < 0.001, n.s., not significant.

significant difference was observed between the two groups (Figs. S3d and e). Additionally, mRNA expressions of *Acox1* and *Cpt1a* were higher in the liver of *Dyrk1b*$^{-/-}$ mice (Fig. S3f). Whereas, the mRNA expressions of *G6pc*, *Gys2*, *Pygl*, *Acaca*, *Fasn*, or *Pnpla2* in liver were not significantly different between female *Dyrk1b*$^{-/-}$ and WT littermates (Fig. S3f).

Male *Dyrk1b*$^{-/-}$ mice did not show any significant alteration of glucose tolerance or insulin resistance under a NCD (Figs. S3g and h). Nevertheless, when challenged with a high-fat diet (HFD) from 6 weeks of age, male *Dyrk1b*$^{-/-}$ mice showed improved glucose tolerance compared to WT littermates (Fig. 3h–j). In the ITT, *Dyrk1b*$^{-/-}$ mice had significantly lower glucose levels at 120 min after insulin injection (Fig. 3k). These data overall suggest that ablation of Dyrk1b can improve systemic glucose metabolism and liver insulin sensitivity in mice.

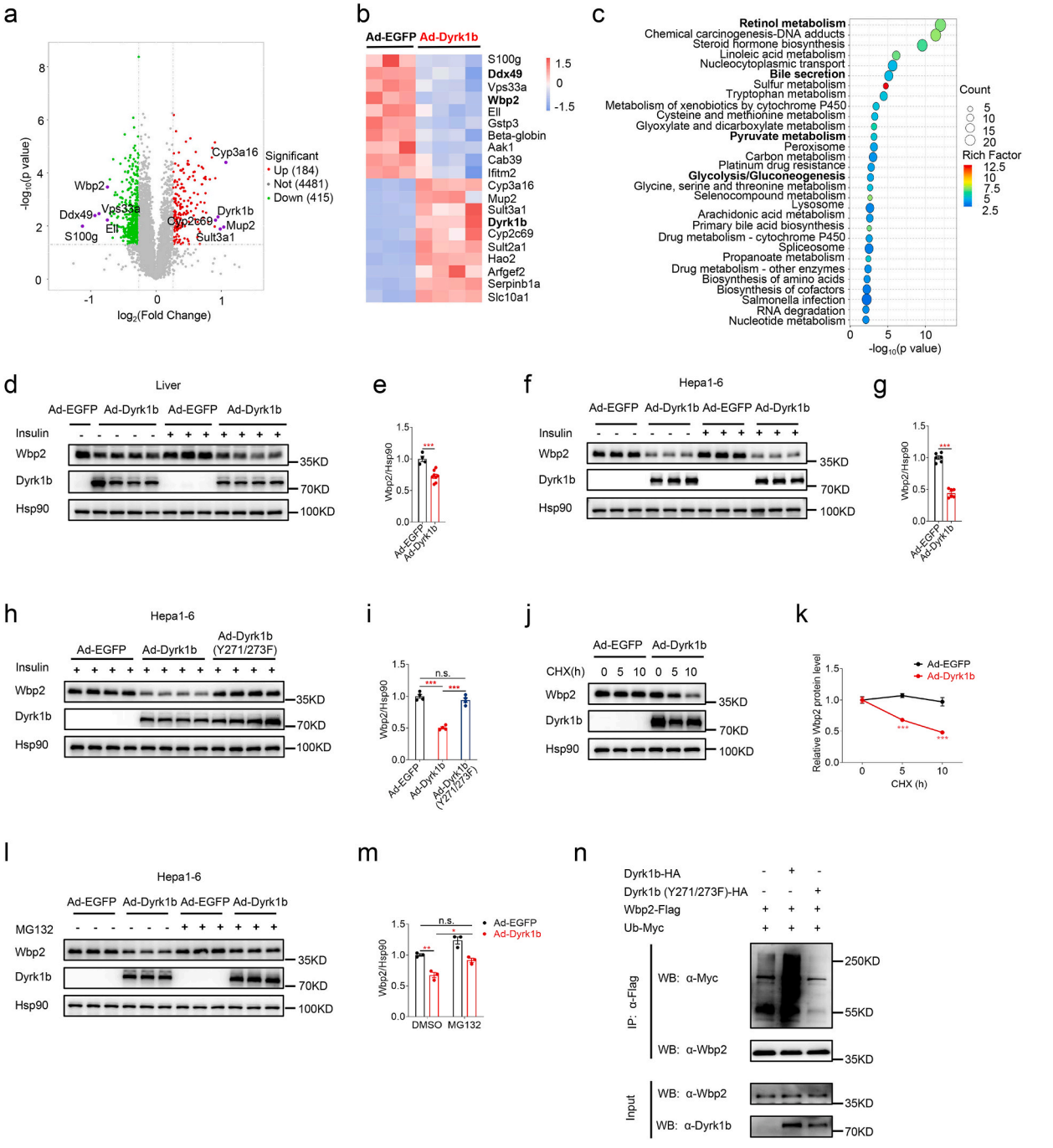

(caption on next page)

Fig. 4. Dyrk1b downregulates Wbp2 protein abundance. (**a**) Volcano plot of differentially expressed proteins between livers of Ad-EGFP (n = 3) and Ad-Dyrk1b (n = 4) female mice. (**b**) Heatmap of the top 20 differentially expressed proteins between livers of Ad-EGFP (n = 3) and Ad-Dyrk1b (n = 4) female mice. (**c**) The top 30 enriched KEGG pathways of differentially expressed proteins between livers of Ad-EGFP (n = 3) and Ad-Dyrk1b (n = 4) female mice. (**d**–**e**) Western blot and densitometry quantification of Wbp2 in livers of Ad-EGFP (n = 4) and Ad-Dyrk1b (n = 8) female mice. Unpaired Student's t-test (two-sided) was performed for Fig. 4**e**. (**f**–**g**) Western blot and densitometry quantification of Wbp2 in Hepa1-6 cells infected with Ad-EGFP or Ad-Dyrk1b (n = 6). Unpaired Student's t-test (two-sided) was performed for Fig. 4**g**. (**h**–**i**) Western blot and densitometry quantification of Wbp2 in Hepa1-6 cells infected with adenovirus expressing wild-type or kinase-defective Dyrk1b (n = 4). One-way ANOVA with Tukey's post-hoc test was performed for Fig. 4**i**. (**j**–**k**) Representative Western blot and densitometry quantification of Wbp2 in Hepa1-6 cells infected with Ad-EGFP or Ad-Dyrk1b and treated with cycloheximide (20 μg/ml) for the indicated time points (n = 4). Unpaired Student's t-test (two-sided) was performed for Fig. 4**k**. (**l**–**m**) Western blot and densitometry quantification of Wbp2 in Hepa1-6 cells infected with Ad-EGFP or Ad-Dyrk1b in the absence or presence of MG132 (5 μM, 4 h) (n = 3). Two-way ANOVA with Tukey's post-hoc test was performed for Fig. 4**m**. (**n**) HA-tagged wild-type or kinase-defective Dyrk1b was expressed in Hepa1-6 cells together with Wbp2-Flag and Ub-Myc. At 45 h post-transfection, cells were treated with MG132 (20 μM) for 3 h and levels of Wbp2 ubiquitylation were evaluated by immunoprecipitation of Wbp2 using anti-Flag antibody followed by anti-Myc immunoblotting. *P < 0.05, **P < 0.01, ***P < 0.001, n.s., not significant.

3.4. Dyrk1b downregulates Wbp2 protein abundance

To elucidate the underlying mechanisms of Dyrk1b in the regulation of glucose homeostasis and to screen the downstream targets of Dyrk1b, we performed a tandem mass tag (TMT)-based quantitative proteomic analysis [39] in the livers of Dyrk1b overexpressing and control female mice. A total of 599 differentially expressed proteins ($p < 0.05$, fold change >1.2 or < 0.83) were identified in the livers of Dyrk1b overexpression mice, of which 184 proteins were upregulated and 415 proteins were downregulated (Fig. 4a). The top 10 upregulated and downregulated proteins were displayed in Fig. 4b. KEGG enrichment analyses of the differentially expressed proteins showed that retinol metabolism, bile secretion, pyruvate metabolism, and glycolysis/gluconeogenesis were among the significantly enriched pathways (Fig. 4c).

We then examined the protein levels of WW domain-binding protein 2 (Wbp2) and Ddx49 by Western blotting and confirmed the significant downregulation of Wbp2 (Fig. 4d and e), but not Ddx49 (Figs. S4a and b), in livers of Dyrk1b overexpression mice. As reported [42], hepatocyte-specific Wbp2 overexpression alleviates glucose tolerance and insulin resistance induced by HFD, while hepatocyte-specific Wbp2 knockdown aggravates HFD-induced glucose tolerance and insulin resistance. We further revealed that Wbp2 protein was also downregulated in Hepa1-6 cells (Fig. 4f and g) and primary hepatocytes overexpressing Dyrk1b (Figs. S4c and d). Despite the decreased Wbp2 protein levels, *Wbp2* mRNA levels were not affected in these cells (Figs. S4e and f). These results suggested that Dyrk1b did not downregulate Wbp2 protein levels via transcriptional regulation.

The downregulation of Wbp2 protein level caused by Dyrk1b overexpression in Hepa1-6 cells was reversed by treatment with AZ191 (Figs. S4g and h). Moreover, kinase-defective Dyrk1b failed to downregulate Wbp2 protein levels in Hepa1-6 cells (Fig. 4h and i) or livers overexpressing kinase-defective Dyrk1b (Figs. S4i and j). These findings demonstrate the requirement of Dyrk1b kinase activity in the regulation of Wbp2. We next assessed the effect of Dyrk1b overexpression on the protein stability of Wbp2. CHX chase assays [35] showed that Dyrk1b overexpression accelerated the degrading speed of Wbp2 (Fig. 4j and k), indicating that Dyrk1b promotes Wbp2 degradation. Notably, treatment with proteasome inhibitor MG132 (Fig. 4l and m) [43], but not lysosome inhibitor Chloroquine (CQ) (Figs. S4k and l) [44], prevented Dyrk1b-induced Wbp2 downregulation. Furthermore, we observed that wild-type Dyrk1b, but not kinase-defective Dyrk1b, increased the level of Wbp2 ubiquitylation (Fig. 4n). These results suggest that Dyrk1b enhances Wbp2 ubiquitylation and promotes its proteasomal degradation.

3.5. Restoration of hepatic Wbp2 expression rescues the impaired glucose homeostasis of Dyrk1b overexpressing mice

Given the role of hepatocyte Wbp2 in glucose metabolism [42] and its downregulation by Dyrk1b, we hypothesized that hepatic Wbp2 downregulation might contribute to the glucose metabolic phenotypes conferred by Dyrk1b overexpression. To test this hypothesis, we firstly examined whether hepatic Wbp2 overexpression through injection of adenovirus expressing Wbp2 could improve the glucose homeostasis of female mice on NCD (Fig. 5a). As expected, hepatic Wbp2 overexpression improved the insulin sensitivity and glucose tolerance of mice (Fig. 5b–e). Significantly increased insulin-stimulated p-Akt at both Thr308 and Ser473 was observed in livers of Wbp2 overexpression mice (Fig. 5f–h). Then, we determined whether restoration of liver Wbp2 expression could rescue glucose metabolic phenotypes in Dyrk1b overexpression mice. Adenovirus expressing Wbp2 and adenovirus expressing Dyrk1b were simultaneously injected into mice to restore Wbp2 expression (Fig. 5i). As a consequence, Wbp2 restoration in liver improved the impaired glucose tolerance caused by Dyrk1b overexpression (Fig. 5j and k). The deteriorated insulin tolerance observed in Dyrk1b overexpression mice was also rescued by hepatic Wbp2 restoration (Fig. 5l and m). Western blotting showed that restoration of hepatic Wbp2 expression recovered the attenuated insulin signaling of Dyrk1b overexpression mice (Fig. 5n and o). Based on these findings, we conclude that hepatic Wbp2 partly mediates the effect of hepatic Dyrk1b overexpression on systemic glucose tolerance and insulin resistance.

3.6. Dyrk1b inhibition moderately ameliorates systemic glucose homeostasis

To further explore the clinical relevance of our findings, we evaluated the effects of Dyrk1b inhibition by AZ191 on glucose metabolism of female C57 mice fed with HFD. Mice were intraperitoneally injected with AZ191 (1.5 mg/kg b.w.) daily for 3 weeks

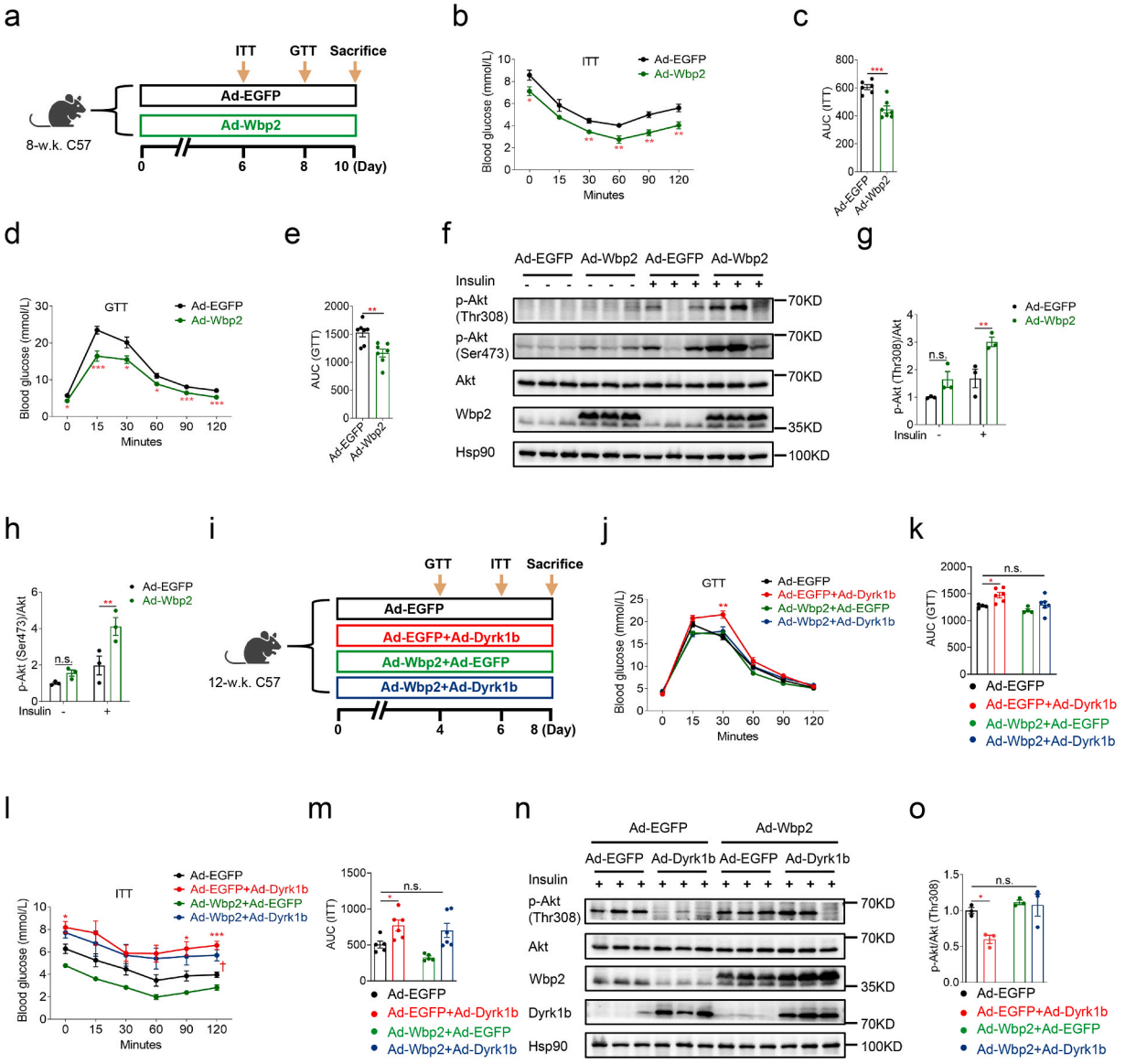

Fig. 5. Restoration of hepatic Wbp2 expression rescues the impaired glucose homeostasis of Dyrk1b overexpressing mice. (**a**) Experimental designs following Ad-Wbp2 or Ad-EGFP injection of female C57 mice. Insulin tolerance test (**b**) and AUC of ITT curves (**c**) of Ad-EGFP (n = 6) and Ad-Wbp2 female mice (n = 7). Glucose tolerance test (**d**) and AUC of GTT curves (**e**) of Ad-EGFP and Ad-Wbp2 female mice (n = 7). Unpaired Student's t-test (two-sided) was performed for Fig. 5**b–e**. (**f-h**) Western blot and densitometry quantification of livers from Ad-EGFP and Ad-Wbp2 female mice. Two-way ANOVA with Sidak's post-hoc test was performed for Fig. 5**g–h**. (**i**) Experimental designs following Ad-Dyrk1b and Ad-Wbp2 injection of female C57 mice. Glucose tolerance test (**j**) and AUC of GTT curves (**k**) of female C57 mice injected with Ad-Dyrk1b and Ad-Wbp2 adenoviruses (n = 4–6). Insulin tolerance test (**l**) and AUC of ITT curves (**m**) of female C57 mice injected with Ad-Dyrk1b and Ad-Wbp2 adenoviruses (n = 5–6). Two-way ANOVA with Dunnett's post-hoc test was performed for Fig. 5**j–m**. *P < 0.05 and ***P < 0.001 for mice injected with Ad-EGFP versus Ad-EGFP and Ad-Dyrk1b, †P < 0.05 for mice injected with Ad-EGFP versus Ad-Dyrk1b and Ad-Wbp2, n.s., not significant. (**n–o**) Western blot and densitometry quantification of p-Akt in livers of female C57 mice injected with Ad-Dyrk1b and Ad-Wbp2 adenoviruses (n = 3). Two-way ANOVA with Dunnett's post-hoc test was performed for Fig. 5**o**. *P < 0.05, **P < 0.01, ***P < 0.001, n.s., not significant.

(Fig. 6a). During the ITT, no significant alternation of insulin sensitivity was observed in mice treated with AZ191 (Fig. 6b). In the GTT, mice treated with AZ191 had significantly lower glucose levels at 60 min after glucose injection (Fig. 6c). Interestingly, a recent study also showed that oral delivery of AZ Dyrk1B 33, a potent Dyrk inhibitor, improved glucose clearance in diabetic db/db mice [45]. Levels of plasma AST, TG, or TC were not affected by AZ191 administration (Fig. 6d–f). Whereas, AZ191 administration decreased plasma HDL-C and LDL-C of mice (Fig. 6g and h). Moreover, AZ191 treatment significantly enhanced levels of insulin-induced p-Akt at both Thr308 and Ser473 in the livers (Fig. 6i–k). These results show that Dyrk1b inhibition by AZ191 moderately ameliorates systemic

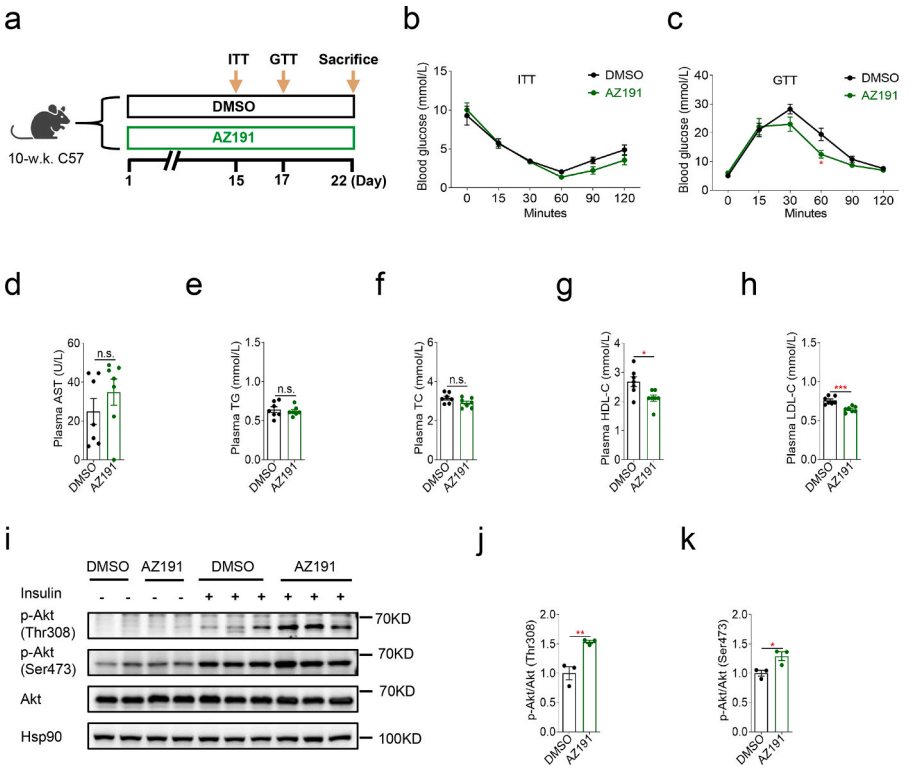

Fig. 6. Dyrk1b inhibition moderately ameliorates systemic glucose homeostasis. (**a**) Experimental designs following DMSO or AZ191 administration of female C57 mice. (**b**) Insulin tolerance test of mice treated with AZ191 or DMSO (n = 6). (**c**) Intraperitoneal glucose tolerance test of mice treated with AZ191 or DMSO (n = 7). (**d-h**) Plasma AST, TG, TC, HDL-C, and LDL-C of mice treated with AZ191 or DMSO (n = 7). Unpaired Student's t-test (two-sided) was performed for Fig. 6**b**–**h**. (**i**–**k**) Western blot and densitometry quantification of p-Akt in livers of mice treated with AZ191 or DMSO (n = 3). Unpaired Student's t-test (two-sided) was performed for Fig. 6**j** and **k**. *P < 0.05, **P < 0.01, ***P < 0.001, n.s., not significant.

glucose tolerance and hepatic insulin signaling.

4. Discussion

In this study, we investigate the role of Dyrk1b in glucose homeostasis. We find that hepatic Dyrk1b overexpression in mice leads to obviously impaired systemic glucose tolerance, increased liver TG, and attenuated insulin signaling in the liver. During the preparation of our manuscript, Bhat et al. demonstrate that Dyrk1b promotes hepatic lipogenesis by activating mTOR2 and causes insulin resistance by impairing insulin receptor kinase activity [41]. It is noteworthy that the authors observe no effect of Dyrk1b overexpression on systemic glucose tolerance. In their study, the authors use AAV8 to increase *Dyrk1b* mRNA by 2-fold. Herein, we overexpress mouse Dyrk1b with adenovirus. The relatively higher hepatic Dyrk1b expression (as shown in Fig. 1i, Fig. S1b, and Fig. S2g) in our study may partially explain the discordant results regarding glucose tolerance. We find that Dyrk1b overexpression in vitro is sufficient to inhibit glucose uptake and canonical insulin signaling of Hepa1-6 cells. AZ191 treatment reverses the inhibition of insulin-stimulated p-Akt caused by Dyrk1b overexpression. In contrast to wild-type Dyrk1b, kinase-defective Dyrk1b fails to inhibit insulin signaling. These data indicate that Dyrk1b antagonizes insulin signaling in a kinase activity-dependent manner. Furthermore, kinase-defective Dyrk1b shows no effect on systemic glucose tolerance or hepatic insulin signaling in vivo, underscoring the importance of the kinase activity of Dyrk1b in its role in glucose homeostasis.

Global ablation of Dyrk1b improves systemic glucose tolerance in female mice on a NCD and male mice on a HFD, but not in male mice maintained on a NCD. The reason for the discrepancy between the phenotypes of male and female *Dyrk1b*$^{-/-}$ mice remains unclear. Since global *Dyrk1b*$^{-/-}$ mice are used in our study, we cannot exclude the possibility that some phenotypes related to glucose metabolism are due to Dyrk1b's role in extra-hepatic tissues. This issue can be addressed by using mice with conditional Dyrk1b knockout in hepatocytes.

TMT-based quantitative proteomic is performed to screen the downstream targets of Dyrk1b. Wbp2 protein abundance is consistently decreased in mice, Hepa1-6 cells, and primary hepatocytes overexpressing Dyrk1b. Dyrk1b overexpression does not impact *Wbp2* mRNA levels in Hepa1-6 cells or primary hepatocytes. CHX chase assays show that Dyrk1b promotes the degradation of Wbp2 protein. Moreover, we find that wild-type Dyrk1b enhances Wbp2 ubiquitylation. One previous study has shown that Wbp2 levels are regulated by ITCH, which targets Wbp2 for ubiquitin-dependent proteasomal degradation [44]. It is possible that Dyrk1b downregulates Wbp2 levels by affecting ITCH-mediated degradation of Wbp2. The precise mechanisms underlying downregulation of

Wbp2 protein level by Dyrk1b remain to be elucidated.

Restoration of hepatic Wbp2 expression partially rescues the impaired glucose tolerance and insulin sensitivity of Dyrk1b overexpression mice. It is likely that some other differentially expressed proteins identified in our the proteomic analyses may also mediate the role of Dyrk1b in glucose metabolism.

Lastly, we find that Dyrk1b inhibition by intraperitoneal AZ191 injection moderately ameliorates glucose metabolism of mice, implying the therapeutic potential of Dyrk1b inhibition in diabetes and metabolic diseases. Our previous study has shown that pharmacological Dyrk1b inhibition with AZ191 elicits morphological and functional benefits for cardiac hypertrophy [23]. These findings indicate the significance of developing specific Dyrk1b inhibitors in the future.

5. Conclusions

In summary, our study uncovers that hepatic Dyrk1b impairs systemic glucose homeostasis via its downregulation of Wbp2 expression in a kinase activity-dependent manner. Our findings will advance the understanding of the mechanisms of glycemic control. Hepatic Dyrk1b may become a potential treatment target for T2DM in the future.

Ethics statement

This study was reviewed and approved by the Animal Care Committee of Shanghai Jiao Tong University School of Medicine with the approval number: B-2016-016.

Funding

This work was supported by grants from the National Key Research and Development Program of China (2022YFC2505201 and 2021YFA1301103), the National Natural Science Foundation of China (82200943, 92157204, 91957124, 82088102, 82250901, and 81930021), the Outstanding Academic Leader Program of Shanghai Municipal Health Commission (2018BR01), and the Program of Shanghai Academic/Technology Research Leader (20XD1403200 and 23XD1422400).

Data availability statement

The proteomic data associated with our study have been deposited to the ProteomeXchange Consortium (http://proteomecentral.proteomexchange.org) with the dataset identifier PXD042393.

CRediT authorship contribution statement

Lianju Li: Writing – original draft, Validation, Software, Methodology, Data curation. **Yaoyu Zou:** Methodology, Funding acquisition, Formal analysis. **Chongrong Shen:** Methodology, Investigation, Formal analysis. **Na Chen:** Software, Methodology, Investigation, Formal analysis. **Muye Tong:** Software, Methodology, Investigation, Formal analysis. **Ruixin Liu:** Supervision, Funding acquisition, Data curation. **Jiqiu Wang:** Supervision, Funding acquisition, Data curation, Conceptualization. **Guang Ning:** Writing – review & editing, Supervision, Funding acquisition, Conceptualization.

Declaration of competing interest

The authors declare that they have no known competing financial interests or personal relationships that could have appeared to influence the work reported in this paper.

Appendix A. Supplementary data

Supplementary data to this article can be found online at https://doi.org/10.1016/j.heliyon.2024.e36726.

References

[1] M. Roden, G.I. Shulman, The integrative biology of type 2 diabetes, Nature 576 (7785) (2019) 51–60.
[2] Y. Zheng, S.H. Ley, F.B. Hu, Global aetiology and epidemiology of type 2 diabetes mellitus and its complications, Nat. Rev. Endocrinol. 14 (2) (2018) 88–98.
[3] A.L. Gloyn, D.J. Drucker, Precision medicine in the management of type 2 diabetes, Lancet Diabetes Endocrinol. 6 (11) (2018) 891–900.
[4] K. Sharabi, C.D. Tavares, A.K. Rines, P. Puigserver, Molecular pathophysiology of hepatic glucose production, Mol. Aspect. Med. 46 (2015) 21–33.
[5] H.V. Lin, D. Accili, Hormonal regulation of hepatic glucose production in health and disease, Cell Metabol. 14 (1) (2011) 9–19.
[6] M.A. Nauck, J. Wefers, J.J. Meier, Treatment of type 2 diabetes: challenges, hopes, and anticipated successes, Lancet Diabetes Endocrinol. 9 (8) (2021) 525–544.
[7] S. Chatterjee, K. Khunti, M.J. Davies, Type 2 diabetes, Lancet 389 (10085) (2017) 2239–2251.
[8] A.L. Ashford, D. Oxley, J. Kettle, K. Hudson, S. Guichard, S.J. Cook, P.A. Lochhead, A novel DYRK1B inhibitor AZ191 demonstrates that DYRK1B acts independently of GSK3β to phosphorylate cyclin D1 at Thr(286), not Thr(288), Biochem. J. 457 (1) (2014) 43–56.

[9] S. Himpel, P. Panzer, K. Eirmbter, H. Czajkowska, M. Sayed, L.C. Packman, T. Blundell, H. Kentrup, J. Grötzinger, H.G. Joost, W. Becker, Identification of the autophosphorylation sites and characterization of their effects in the protein kinase DYRK1A, Biochem. J. 359 (Pt 3) (2001) 497–505.

[10] P.A. Lochhead, G. Sibbet, N. Morrice, V. Cleghon, Activation-loop autophosphorylation is mediated by a novel transitional intermediate form of DYRKs, Cell 121 (6) (2005) 925–936.

[11] X. Deng, D.Z. Ewton, S.E. Mercer, E. Friedman, Mirk/dyrk1B decreases the nuclear accumulation of class II histone deacetylases during skeletal muscle differentiation, J. Biol. Chem. 280 (6) (2005) 4894–4905.

[12] S.E. Mercer, D.Z. Ewton, X. Deng, S. Lim, T.R. Mazur, E. Friedman, Mirk/Dyrk1B mediates survival during the differentiation of C2C12 myoblasts, J. Biol. Chem. 280 (27) (2005) 25788–25801.

[13] S.E. Mercer, D.Z. Ewton, S. Shah, A. Naqvi, E. Friedman, Mirk/Dyrk1b mediates cell survival in rhabdomyosarcomas, Cancer Res. 66 (10) (2006) 5143–5150.

[14] X. Deng, D.Z. Ewton, S. Li, A. Naqvi, S.E. Mercer, S. Landas, E. Friedman, The kinase Mirk/Dyrk1B mediates cell survival in pancreatic ductal adenocarcinoma, Cancer Res. 66 (8) (2006) 4149–4158.

[15] C. Dong, K.L. West, X.Y. Tan, J. Li, T. Ishibashi, C.H. Yu, S.M.H. Sy, J.W.C. Leung, M.S.Y. Huen, Screen identifies DYRK1B network as mediator of transcription repression on damaged chromatin, Proc. Natl. Acad. Sci. U. S. A 117 (29) (2020) 17019–17030.

[16] C. Dong, L. An, C.H. Yu, M.S.Y. Huen, A DYRK1B-dependent pathway suppresses rDNA transcription in response to DNA damage, Nucleic Acids Res. 49 (3) (2021) 1485–1496.

[17] C. Yang, D. Ji, E.J. Weinstein, E. Choy, F.J. Hornicek, K.B. Wood, X. Liu, H. Mankin, Z. Duan, The kinase Mirk is a potential therapeutic target in osteosarcoma, Carcinogenesis 31 (4) (2010) 552–558.

[18] J. Gao, Z. Zheng, B. Rawal, M.J. Schell, G. Bepler, E.B. Haura, Mirk/Dyrk1B, a novel therapeutic target, mediates cell survival in non-small cell lung cancer cells, Cancer Biol. Ther. 8 (17) (2009) 1671–1679.

[19] C.C. Chang, C.C. Chiu, P.F. Liu, C.H. Wu, Y.C. Tseng, C.H. Lee, C.W. Shu, Kinome-wide siRNA screening identifies DYRK1B as a potential therapeutic target for triple-negative breast cancer cells, Cancers 13 (22) (2021) 5779.

[20] W. Becker, A wake-up call to quiescent cancer cells - potential use of DYRK1B inhibitors in cancer therapy, FEBS J. 285 (7) (2018) 1203–1211.

[21] J. Boni, C. Rubio-Perez, N. López-Bigas, C. Fillat, S. de la Luna, The DYRK family of kinases in cancer: molecular functions and therapeutic opportunities, Cancers 12 (8) (2020) 2106.

[22] J. Zhao, Y. Xu, J. Wang, J. Liu, R. Zhang, X. Yan, Dual-specificity tyrosine phosphorylation-regulated kinase 1B inhibition promotes megakaryocyte polyploidization and platelet production, Thromb. Haemostasis 123 (2) (2023) 192–206.

[23] L. Zhuang, K. Jia, C. Chen, Z. Li, J. Zhao, J. Hu, H. Zhang, Q. Fan, C. Huang, H. Xie, L. Lu, W. Shen, G. Ning, J. Wang, R. Zhang, K. Chen, X. Yan, DYRK1B-STAT3 drives cardiac hypertrophy and heart failure by impairing mitochondrial bioenergetics, Circulation 145 (11) (2022) 829–846.

[24] A.R. Keramati, M. Fathzadeh, G.W. Go, R. Singh, M. Choi, S. Faramarzi, S. Mane, M. Kasaei, K. Sarajzadeh-Fard, J. Hwa, K.K. Kidd, M.A. Babaee Bigi, R. Malekzadeh, A. Hosseinian, M. Babaei, R.P. Lifton, A. Mani, A form of the metabolic syndrome associated with mutations in DYRK1B, N. Engl. J. Med. 370 (20) (2014) 1909–1919.

[25] J. Boch, H. Scholze, S. Schornack, A. Landgraf, S. Hahn, S. Kay, T. Lahaye, A. Nickstadt, U. Bonas, Breaking the code of DNA binding specificity of TAL-type III effectors, Science 326 (5959) (2009) 1509–1512.

[26] N. Tatsis, H.C. Ertl, Adenoviruses as vaccine vectors, Mol. Ther. 10 (4) (2004) 616–629.

[27] A. Gao, J. Su, R. Liu, S. Zhao, W. Li, X. Xu, D. Li, J. Shi, B. Gu, J. Zhang, Q. Li, X. Wang, Y. Zhang, Y. Xu, J. Lu, G. Ning, J. Hong, Y. Bi, W. Gu, J. Wang, W. Wang, Sexual dimorphism in glucose metabolism is shaped by androgen-driven gut microbiome, Nat. Commun. 12 (1) (2021) 7080.

[28] J. Wang, R. Liu, F. Wang, J. Hong, X. Li, M. Chen, Y. Ke, X. Zhang, Q. Ma, R. Wang, J. Shi, B. Cui, W. Gu, Y. Zhang, Z. Zhang, W. Wang, X. Xia, M. Liu, G. Ning, Ablation of LGR4 promotes energy expenditure by driving white-to-brown fat switch, Nat. Cell Biol. 15 (12) (2013) 1455–1463.

[29] M. Xiang, X. Qian, L. Han, H. Wang, J. Wang, W. Liu, Y. Gu, S. Yao, J. Yang, Y. Zhang, Y. Peng, Z. Zhang, Aquaporin-8 ameliorates hepatic steatosis through farnesoid X receptor in obese mice, iScience 26 (4) (2023) 106561.

[30] S.Y. Jiang, J.J. Tang, X. Xiao, et al., Schnyder corneal dystrophy-associated UBIAD1 mutations cause corneal cholesterol accumulation by stabilizing HMG-CoA reductase, PLoS Genet. 15 (7) (2019) e1008289.

[31] M.P. Valley, N. Karassina, N. Aoyama, C. Carlson, J.J. Cali, J. Vidugiriene, A bioluminescent assay for measuring glucose uptake, Anal. Biochem. 505 (2016) 43–50.

[32] N. Chen, M. Yuan, N. Zhang, M. Chen, R. Liu, J. Wang, P. Lu, Ctnnb1/β-catenin inactivation in UCP1-positive adipocytes augments the browning of white adipose tissue, iScience 26 (5) (2023) 106552.

[33] K.J. Livak, T.D. Schmittgen, Analysis of relative gene expression data using real-time quantitative PCR and the 2(-Delta Delta C(T)) Method, Methods 25 (4) (2001) 402–408.

[34] Y. Sun, J. Zhang, J. Hong, Z. Zhang, P. Lu, A. Gao, M. Ni, Z. Zhang, H. Yang, J. Shen, J. Lu, W. Xue, Q. Lv, Y. Bi, Y.A. Zeng, W. Gu, G. Ning, W. Wang, R. Liu, J. Wang, Human RSPO1 mutation represses beige adipocyte thermogenesis and contributes to diet-induced adiposity, Adv. Sci. 10 (12) (2023) e2207152.

[35] X. Zhao, D. Shu, W. Sun, S. Si, W. Ran, B. Guo, L. Cui, PLEK2 promotes cancer stemness and tumorigenesis of head and neck squamous cell carcinoma via the c-Myc-mediated positive feedback loop, Cancer Commun. 42 (10) (2022) 987–1007.

[36] L. Li, J. Fu, D. Liu, J. Sun, Y. Hou, C. Chen, J. Shao, L. Wang, X. Wang, R. Zhao, H. Wang, M.E. Andersen, Q. Zhang, Y. Xu, J. Pi, Hepatocyte-specific Nrf2 deficiency mitigates high-fat diet-induced hepatic steatosis: involvement of reduced PPARγ expression, Redox Biol. 30 (2020) 101412.

[37] P. Sampathkumar, H. Jung, H. Chen, Z. Zhang, N. Suen, Y. Yang, Z. Huang, T. Lopez, R. Benisch, S.J. Lee, J. Ye, W.C. Yeh, Y. Li, Targeted protein degradation systems to enhance Wnt signaling, Elife 13 (2024) RP93908.

[38] S. Zhao, W. Liu, J. Wang, J. Shi, Y. Sun, W. Wang, G. Ning, R. Liu, J. Hong, Akkermansia muciniphila improves metabolic profiles by reducing inflammation in chow diet-fed mice, J. Mol. Endocrinol. 58 (1) (2017) 1–14.

[39] J.A. Ankney, A. Muneer, X. Chen, Relative and absolute quantitation in mass spectrometry-based proteomics, Annu. Rev. Anal. Chem. 11 (1) (2018) 49–77.

[40] J.R. Wiśniewski, A. Zougman, N. Nagaraj, M. Mann, Universal sample preparation method for proteome analysis, Nat. Methods 6 (5) (2009) 359–362.

[41] N. Bhat, A. Narayanan, M. Fathzadeh, M. Kahn, D. Zhang, L. Goedeke, A. Neogi, R.L. Cardone, R.G. Kibbey, C. Fernandez-Hernando, H.N. Ginsberg, D. Jain, G. I. Shulman, A. Mani, Dyrk1b promotes hepatic lipogenesis by bypassing canonical insulin signaling and directly activating mTORC2 in mice, J. Clin. Invest. 132 (3) (2022) e153724.

[42] Z. Zheng, Y. Li, S. Fan, J. An, X. Luo, M. Liang, F. Zhu, K. Huang, WW domain-binding protein 2 overexpression prevents diet-induced liver steatosis and insulin resistance through AMPKβ1, Cell Death Dis. 12 (3) (2021) 228.

[43] J. Meng, X. Ai, Y. Lei, W. Zhong, B. Qian, K. Qiao, X. Wang, B. Zhou, H. Wang, L. Huai, X. Zhang, J. Han, Y. Xue, Y. Liang, H. Zhou, S. Chen, T. Sun, C. Yang, USP5 promotes epithelial-mesenchymal transition by stabilizing SLUG in hepatocellular carcinoma, Theranostics 9 (2) (2019) 573–587.

[44] S.K. Lim, S.Y. Lu, S.A. Kang, H.J. Tan, Z. Li, Z.N. Adrian Wee, J.S. Guan, V.P. Reddy Chichili, J. Sivaraman, T. Putti, A.A. Thike, P.H. Tan, M. Sudol, D. M. Virshup, S.W. Chan, W. Hong, Y.P. Lim, Wnt signaling promotes breast cancer by blocking ITCH-mediated degradation of YAP/TAZ transcriptional coactivator WBP2, Cancer Res. 76 (21) (2016) 6278–6289.

[45] L. Chu, M. Terasaki, C.L. Mattsson, R. Teinturier, J. Charbord, E. Dirice, K.C. Liu, M.G. Miskelly, Q. Zhou, N. Wierup, R.N. Kulkarni, O. Andersson, In vivo drug discovery for increasing incretin-expressing cells identifies DYRK inhibitors that reinforce the enteroendocrine system, Cell Chem. Biol. 29 (9) (2022) 1368–1380.e5.